IMPRS GW Astronomy – Computational Physics 2025
Hydrodynamics

Takami Kuroda

1 Introduction to GR hydrodynamic equations

In the previous lectures, we have learned several basics on how to numerically evolve the left hand side of Einstein field equations EFE (in the vacuum space)

$$G_{ab}\gamma^a_i\gamma^b_j = 0, \tag{1}$$

satisfying two constraints

$$\begin{aligned} G_{ab}n^a n^b &= 0 \quad \text{Hamiltonian constraint} & (2)\\ G_{ab}n^a\gamma^b_i &= 0 \quad \text{momentum constraint.} & (3)\end{aligned}$$

In the presence of matter (i.e. $T_{ab} \neq 0$), however, we also have to evolve the right hand side of EFE via

$$0 = \nabla_a G^{ab} = 8\pi\nabla_a T^{ab}, \tag{4}$$

which is derived from the Bianchi identity. In addition, the following continuity equation

$$\nabla_a J^a = 0, \tag{5}$$

has to be simultaneously solved. Here J^a denotes the matter current density defined by $J^a = \rho_0 u^a$, with ρ_0 and u^a being the rest mass density and the 4-velocity, respectively. In the 3+1 formalism, we usually project $\nabla_a T^{ab}$ in Eq. (4) parallel to the future normal vector n^a and into the foliated hypersurface as follows:

$$\begin{aligned} n^b\nabla_a T^a_b &= 0 & (6)\\ \gamma^b_i\nabla_a T^a_b &= 0 & (7)\end{aligned}$$

Consequently, the basic hydrodynamic equations to be solved are Eqs. (5), (6), and (7).

1.1 The stress-energy tensor T^{ab} and current density J^a

In the practical problems, we sometimes have to consider various forms of stress-energy tensor and current density. For instance, when we want to solve the binary neutron star or core-collapse supernova (CCSN) simulation, the stress-energy tensor can be consisted of matter, radiation, and electro-magnetic fields. Similarly, the current density should be the mass current, which is basically nearly identical to the number current density of baryons (e.g. neutron, proton, heavy nuclei, etc.), and the lepton number current such

as of free electrons.
In the current lecture, we consider the basic ideal gas assuming barionic matters and described by

$$\begin{aligned} J^a &= \rho_0 u^a & (8)\\ T^{ab} &= \rho_0 h u^a u^b + p g^{ab}. & (9) \end{aligned}$$

Here h and p denote the specific enthalpy and matter pressure, respectively. The specific enthalpy h is expressed by $h = 1 + \varepsilon + p/\rho_0$, with ε being the specific internal energy.

1.2 GR hydrodynamic equations

After plugging Eqs. (8) and (9) into Eqs. (5), (6), and (7), the basic GR hydrodynamic equations can be written as

$$\begin{aligned} \partial_t \rho_* + \partial_i \left(\rho_* v^i\right) &= 0 & (10)\\ \partial_t S_j + \partial_i \left(S_j v^i + \alpha e^{6\phi} p \delta^i_j\right) &= S_{\mathrm{grv,S}} & (11)\\ \partial_t \tau + \partial_i \left[\tau v^i + e^{6\phi} p \left(v^i + \beta^i\right)\right] &= S_{\mathrm{grv},\tau}. & (12) \end{aligned}$$

Here, $\rho_* = \rho_0 W e^{6\phi}$ is a weighted (baryon) rest mass density, with W being the Lorentz factor; $v^i = u^i/u^t$: the three velocity; $S_i = \rho_0 h W u_i e^{6\phi}$: a weighted momentum density; $\tau = (\rho_0 h W^2 - P)e^{6\phi} - \rho_*$: a weighted energy density excluding the rest mass contribution. $S_{\mathrm{grv},S/\tau}$ on the right hand side represents gravitational source terms.
In ODE/PDE lectures, we learned how to solve evolution equations of the form

$$\partial_t y + \partial_x f(x, y) = 0, \tag{13}$$

which is quite similar to the above equations (10)-(12). However, in ODE/PDE lectures, we presumed $f(x, y)$ is continuous at least within an interval considered. Meanwhile, in the practical fluid systems the discontinuity appears quite often. This is the most critical difference between the gravitational field, which is basically smooth and continuous over the spacetime, and the matter stress-energy tensor that sometimes has discontinuities. We, therefore, have to solve the hydrodynamic equations with a special care. To that end, we shall first see the two basic concepts of descretization in space: finite difference and finite volume.

2 Discretization in space: finite difference and finite volume

In ODE/PDE lectures, we learned the finite difference method (FDM), where we discretize the system and evaluate the slope using values defined on those descretized points such as

$$\rho_i = \rho(x_i). \tag{14}$$

Using these *sampled* values, we solve the system from the evaluated slope. For instance Eq. (10) becomes (here after, we assume only the Newtonian limit),

$$\partial_t \rho_i + \frac{\rho_{i+1} v_{i+1} - \rho_{i-1} v_{i-1}}{2\Delta x} = 0, \tag{15}$$

in the 2nd order finite difference method.
On the other hand, in the finite volume method (FVM), one should start with defining all quantities measured at position i (corresponding to spatial index) by volume averaged values: E.g.,

$$\bar{\rho}_i = \frac{\int_{i-\frac{1}{2}}^{i+\frac{1}{2}} dx \rho(x)}{\int_{i-\frac{1}{2}}^{i+\frac{1}{2}} dx}. \tag{16}$$

Here we assume a 1D space, but extension to multi-dimension is straightforward. From this expression, therefore, we can read that physical quantities are assumed to have continuous structures and can be defined at every location x. (Note that the "continuous" here does not mean the structure has to be smooth without discontinuity.) Then Eq. (10) becomes,

$$\partial_t \bar{\rho}_i + \frac{1}{\Delta x} \partial_i \left(\int_{i-\frac{1}{2}}^{i+\frac{1}{2}} dx \rho(x) v(x) \right) = 0, \tag{17}$$

where $\Delta x = \int_{i-1/2}^{i+1/2} dx$. Next step is a conversion of the divergence term appearing in the equation, i.e. $\partial_i(\cdots)$, to surface integral using Gauss's theorem. Explicitly the above equation can be rewritten as

$$\partial_t \bar{\rho}_i + \frac{[\rho(x)v(x)]_{i+\frac{1}{2}} - [\rho(x)v(x)]_{i-\frac{1}{2}}}{\Delta x} = 0. \tag{18}$$

Here $[\dots]_{i+1/2}$ represents the value measured on the surface at $(i + 1/2)$-th position.
Now let's see how a system with discontinuity evolves in two different methods: FDM (e.g. Eq. (15)) and FVM (Eq. 18).

2.1 Simple advection test: FDM

We begin with FDM case. In this test, we solve a simple advection equation of a similar form with Eq. (10)

$$\partial_t \rho + \partial_x (\rho v) = 0, \tag{19}$$

but with $v = const.$, thus

$$\partial_t \rho + v \partial_x \rho = 0. \tag{20}$$

This is a PDE and if we descretize the equation by FDM with 1st order in time and 2nd order in space as follows:

$$\frac{\rho_i^{n+1} - \rho_i^n}{\Delta t} + v \frac{\rho_{i+1}^n - \rho_{i-1}^n}{2\Delta x} = 0, \tag{21}$$

where the upper and lower indices n and i represent the time and space indices, respectively, with $\Delta t(\Delta x)$ being the time(space) step size, we can evaluate the value at

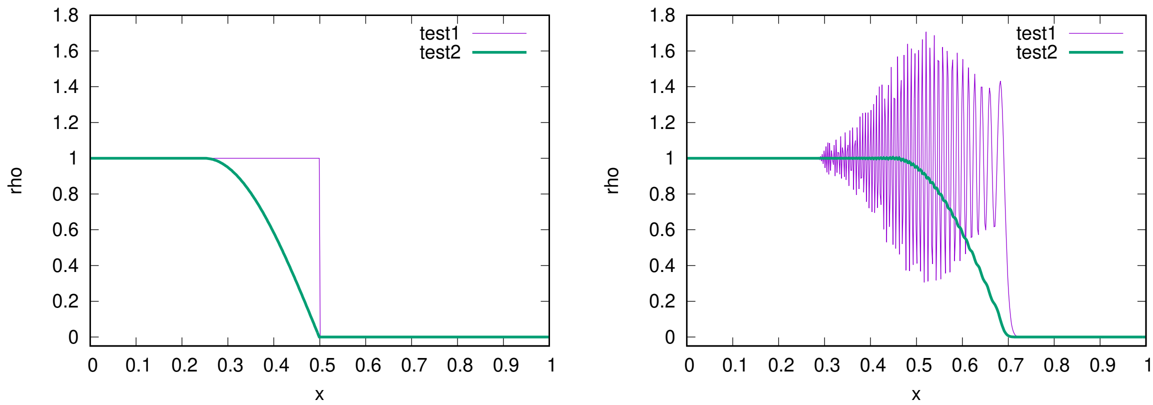

Figure 1: Initial conditions (left panel) and evolved structures at $t = 0.2$ (right panel). We use FDM (Eq. 22). The spatial grid is $\Delta x = 1/500$.

$(n+1)$-th time step as

$$\rho_i^{n+1} = \rho_i^n - v\Delta t \frac{\rho_{i+1}^n - \rho_{i-1}^n}{2\Delta x} = 0. \tag{22}$$

We assume two initial states. One is with a discontinuity at $x = 0.5$ (test 1: purple line in the left panel of Fig. 1)

$$\rho(x) = \begin{cases} 1 & (x \leq 0.5) \\ 0 & (x > 0.5) \end{cases}, \tag{23}$$

the other is with a smooth structure (test 2: green line in the left panel of Fig. 1)

$$\rho(x) = \begin{cases} 1 & (x \leq 0.25) \\ \cos\left(\frac{\pi}{2}\frac{x-0.25}{0.25}\right) & (0.25 < x \leq 0.5) \\ 0 & (x > 0.5) \end{cases}. \tag{24}$$

We evolve these two initial states following Eq. (22). We set the fluid velocity $v = 1$ and the time step is determined by

$$\Delta t = \mathrm{CFL}\frac{\Delta x}{v}, \tag{25}$$

where the Courant–Friedrichs–Lewy number of $\mathrm{CFL} = 0.05$ (to excite the oscillation, I artificially use a small CFL number) is used.
Fig. 1 illustrates the initial conditions (top panel) and evolved structures at $t = 0.2$ (lower panel). The spatial grid is set to be $\Delta x = 1/500$.
From figure, it is obvious that the structure with a discontinuity shows a significant numerical oscillations (purple line) behind the discontinuity at $t = 0.2$, while the initially smooth structure simply advects toward right as expected (green line).

2.2 Simple advection test: FVM

The next test is done by FVM. But before that it may be better to rewrite Eq. (18) as follows.

$$\partial_t \bar{\rho}_i + \frac{f_{i+\frac{1}{2}} - f_{i-\frac{1}{2}}}{\Delta x} = 0. \tag{26}$$

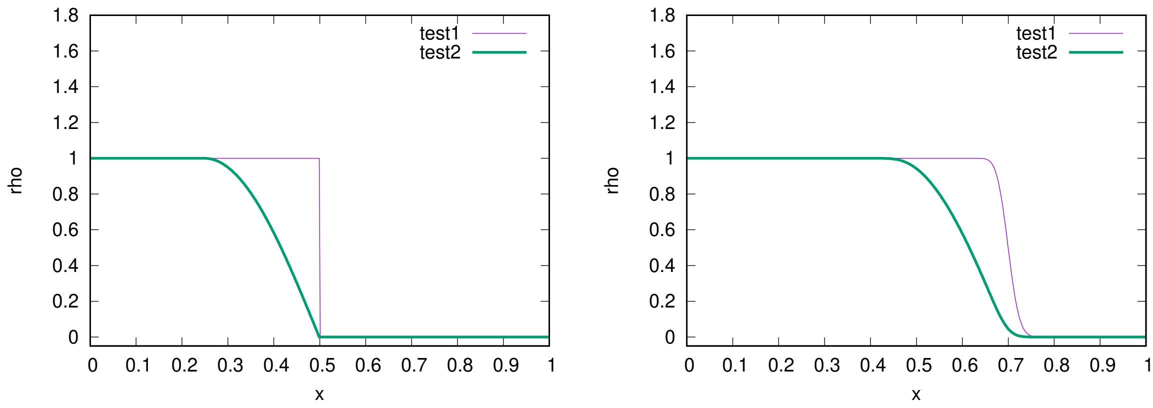

Figure 2: Same with Fig. 1, but with FVM.

We can interpret $f_{i+1/2}$ as a (mass or number in this case) flux penetrating through a surface at $(i+1/2)$-th position. However there appears a problem: How can we appropriately evaluate the flux on the cell surface? As there is no unique definition, we will see a few possible options.

2.2.1 Central scheme

The simplest form might be

$$f_{i+\frac{1}{2}} = \frac{f_i + f_{i+1}}{2}. \tag{27}$$

However if we insert it into Eq. (26), we immediately find that it is identical to Eq. (15) (now $f_i = \rho_i v_i$). Therefore we can safely abandon this option as this is quite unstable method shown by purple line in Fig. 1.

2.2.2 First-order upwind scheme

Next we consider the so-called upwind scheme. The underlying concept is that we should evaluate the surface flux $f_{i+1/2}$ by the value at upstream region. Suppose the entire fluid has a positive velocity $v > 0$, then the i-th position corresponds to the upstream w.r.t. $(i+1/2)$-th location. Thence

$$f_{i+\frac{1}{2}} = f_i \qquad \text{for } v > 0. \tag{28}$$

Analogously

$$f_{i+\frac{1}{2}} = f_{i+1} \qquad \text{for } v < 0. \tag{29}$$

If we apply this upwind scheme to Eq. (26), we obtain

$$\partial_t \bar{\rho}_i + \frac{v^+ (\rho_i - \rho_{i-1}) + v^- (\rho_{i+1} - \rho_i)}{\Delta x} = 0, \tag{30}$$

where $v^+ = \max(v, 0)$ and $v^- = \min(v, 0)$.
Fig. 2 exhibits the same test with Fig. 1, but with FVM using Eq. (30). We can clearly see that the numerical oscillations previously observed in FDM models completely disappeared. Therefore this method is much better than the previous simple central scheme.

However, we find that the initial sharp discontinuity is smeared out (purple line in the right panel). This would become a serious problem if we calculate quite long time.

3 High-order shock capturing schemes

In the previous section, we have discussed that FVM is more effective when dealing with discontinuities, which was proven by a simple 1st order upwind scheme. At the same time, however, the simple 1st order scheme is too diffusive and the initial discontinuous structure is soon smeared out. Therefore we need higher-order schemes that enable us to reconstruct the surface flux $f_{i+1/2}$ more accurately. In doing so, we have to pay attention to several points:

- Accuracy: high-order scheme
- Conservativity: local and global
- Numerical stability: monotonicity

Regarding the first point "Accuracy", it means that we should basically employ higher-order reconstruction schemes as possible: Namely 3rd order is better than 2nd order and 4th order is better than 3rd, and so on. At the same time, however, we should keep in mind that the higher order methods usually require more computational time than lower order methods. Furthermore, the higher order methods are known to often introduce undesired oscillatory behavior, especially behind the shock, which ultimately leads to numerical instability. Such oscillations when entered in the non-linear regime not only cause the numerical instability but also violate the local conservation law, even though the total conservation may be satisfied thanks to the FVM, which evolves the volume averaged quantities by the Gauss's theorem. Like these, we have to avoid such oscillatory behavior during calculations and here we need to consider the "Monotonicity".

3.1 Monotonicity

Monotonicity means that the values are continuously increasing/decreasing or constant over the entire region considered. For instance, in the right panel of Fig. 1, we see many new extrema in purple line, despite the initial condition was monotonic (Eq. 23), which clearly violates the monotonicity preservation. And to avoid such spurious numerical oscillation or overshooting at the discontinuity, monotonicity has to be preserved after every time step, if the initial structure is also monotonic. However, Godunov's theorem (skip its detailed proof) states that any "linear" monotonicity-preserving schemes can be at most first-order accurate. Therefore if we need both higher-order schemes to capture the sharp discontinuity and monotonicity preservation, we have to consider "non-linear" methods.

3.2 PLM scheme

In piecewise linear method (PLM), we reconstruct the boundary value by evaluating a slope in each numerical cell taking into account the propagation direction of the fluid. For instance

$$f_{i+\frac{1}{2}} = \rho_i v_i + \frac{1}{2}\delta(\rho_i v_i)\left[1 - v_i\frac{\Delta t}{\Delta x}\right] \quad \text{for } v_i > 0, \tag{31}$$

and

$$f_{i-\frac{1}{2}} = \rho_i v_i + \frac{1}{2}\delta(\rho_i v_i)\left[1 + v_i \frac{\Delta t}{\Delta x}\right] \quad \text{for } v_i < 0. \tag{32}$$

Here $\delta(\rho_i v_i)$ denotes a slope function. Among several possible slope functions $\delta(\cdot)$, the Lax–Wendroff method employs

$$\delta(X_i) \equiv X_{i+1} - X_i, \tag{33}$$

and is second-order accurate in both space and time. Explicitly the next step value for the equation $\partial_t \rho + \partial_x(\rho v^x) = 0$ is expressed as

$$\begin{aligned} \rho_i^{n+1} &= \rho_i^n - \frac{\Delta t}{\Delta x}\left(f_{i+\frac{1}{2}}^n - f_{i-\frac{1}{2}}^n\right) \\ &= \rho_i^n - \frac{\Delta t}{2\Delta x}(\rho_{i+1}^n v_{i+1}^n - \rho_{i-1}^n v_{i-1}^n) + \frac{\Delta t^2}{2\Delta x^2}(\rho_{i+1}^n v_{i+1}^n - 2\rho_i^n v_i^n + \rho_{i-1}^n v_{i-1}^n). \end{aligned} \tag{34}$$

Now let's compare two schemes: 1st-order upwind scheme Eq. (30) and Lax-Wendroff scheme. Fig. 3 plots a comparison of these two. We see that the Lax-Wendroff scheme can more sharply capture the discontinuity, but at the same time it produces undesirable oscillations.

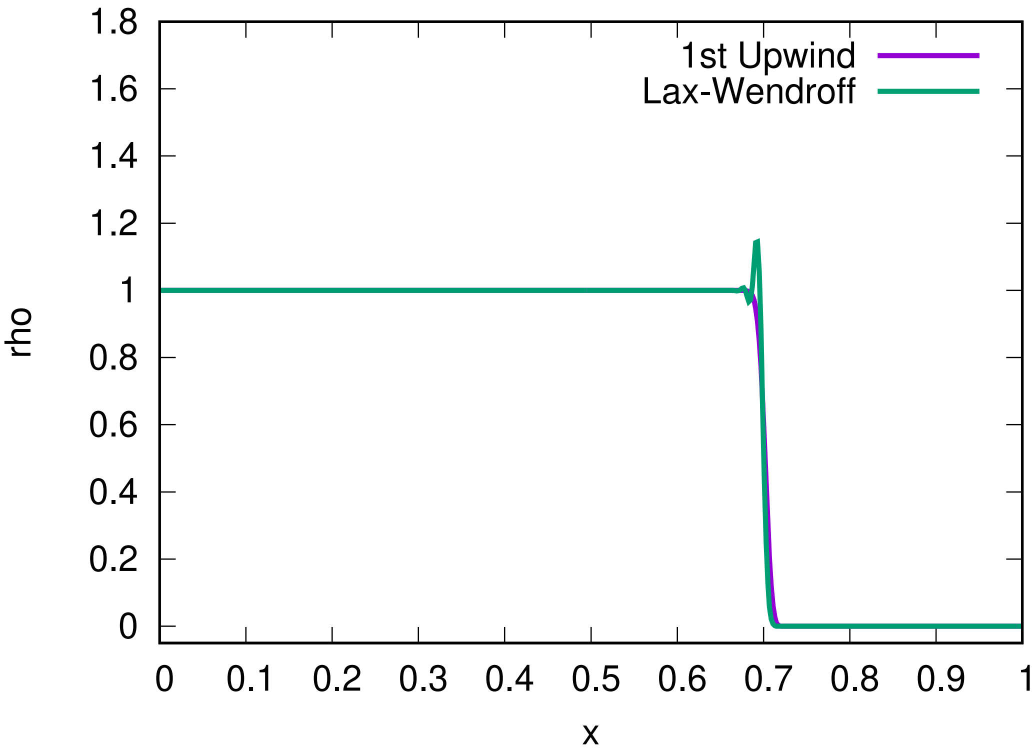

Figure 3: Same with Fig. 1, but with 1st-order upwind scheme (purple, see also Eq. (30)) and Lax-Wendroff scheme (green).

3.3 Flux limiter

To suppress the oscillations we need "flux-limiter" $\phi(r_i)$. We can apply this function for instance as below.

$$f_{i+\frac{1}{2}} = f_i + \frac{1}{2}\phi(r_i)\delta(f_i)\left[1 - v_i\frac{\Delta t}{\Delta x}\right] \quad \text{for } v_i > 0, \tag{35}$$

and

$$f_{i-\frac{1}{2}} = f_i + \frac{1}{2}\phi(r_i)\delta(f_i)\left[1 + v_i\frac{\Delta t}{\Delta x}\right] \quad \text{for } v_i < 0, \tag{36}$$

where

$$r_i \equiv \frac{f_i - f_{i-1}}{f_{i+1} - f_i}. \tag{37}$$

The underlying concept is that if there is too large difference between relevant slopes, e.g. $f_i - f_{i-1}$ and $f_{i+1} - f_i$ as illustrated in Fig. 4, which is often observed across the discontinuity, then we should select a more *reasonable* slope and use that value to estimate the flux $f_{i+1/2}$ at cell surface.

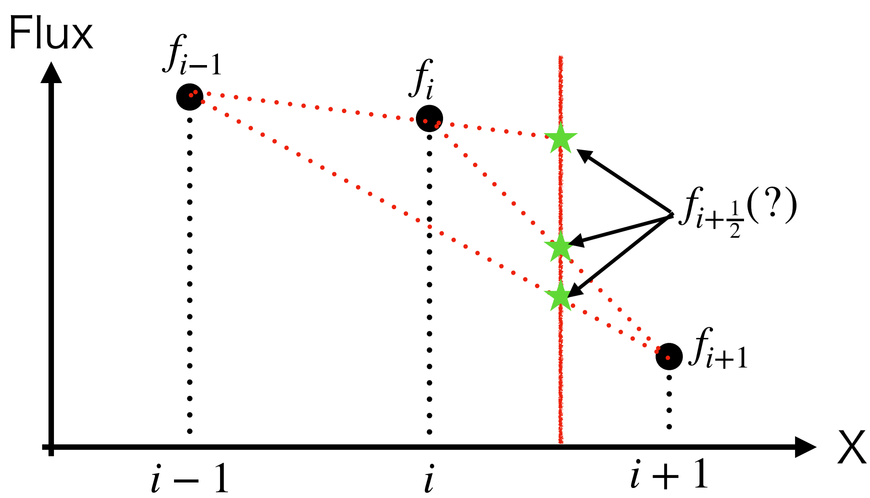

Figure 4: A schematic picture of the concept of flux limiter.

There are indeed a bunch of limiter functions (see Wikipedia), such as CHARM, minmod, monotonized central, superbee, van Leer, etc. As an example, we now see how the "minmod" function works to suppress the oscillation. The limiter function $\phi_{\text{minmod}}(r)$ is defined as

$$\phi_{\text{minmod}}(r) = \max(0, \min(1, r)). \tag{38}$$

If we apply this function, we can evolve the propagation of discontinuity without spurious oscillations, while retaining the sharp discontinuity as shown in Fig. 5.

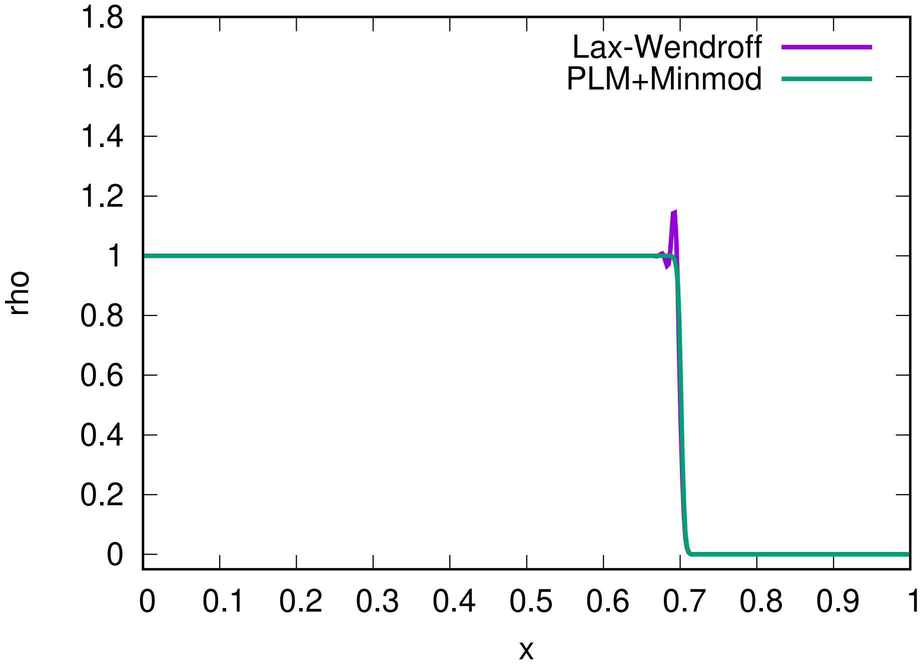

Figure 5: Same with Fig. 3, but with the Lax-Wendroff scheme (purple) and PLM+slope-limiter (Minmod) (green).